NASA TM X-1418

CALCULATION OF FAST-NEUTRON FLUX EMERGING FROM A REACTOR BEAMHOLE AND COMPARISON WITH EXPERIMENT

By Harvey S. Bloomfield

Lewis Research Center
Cleveland, Ohio

NATIONAL AERONAUTICS AND SPACE ADMINISTRATION

For sale by the Clearinghouse for Federal Scientific and Technical Information
Springfield, Virginia 22151 – CFSTI price $3.00

CALCULATION OF FAST-NEUTRON FLUX EMERGING FROM A REACTOR BEAMHOLE AND COMPARISON WITH EXPERIMENT

by Harvey S. Bloomfield

Lewis Research Center

SUMMARY

A comparison of calculated and measured fast-neutron fluxes emerging from the HB-6 beamhole of the NASA Plum Brook reactor is presented. Integrated dose rates were calculated with the QAD line-of-sight computer program using Albert-Welton removal theory to account for neutron attenuation. The program output was converted to fast flux with the Snyder-Neufeld conversion factors and then modified by the use of collimated removal cross sections to account for the reduction of the scattered flux component emerging from the duct. In addition, the use of neutron removal theory in non-hydrogenous media was assumed valid because of recent measurements.

Measured flux values were calculated from sulfur foil activation data and then extrapolated to a lower energy of 0.3 MeV (0.048 picojoule) to correspond to the conventional energy range of the calculational method. The extrapolation was carried out by using both a fission spectrum and a beryllium altered fission spectrum. These spectra were chosen to represent the possible extremes of the true duct spectrum, which was estimated to be a hardened fission spectrum.

Results of the comparison indicate that the calculational method can predict fast-neutron fluxes emerging from the HB-6 beamhole to within a factor of about 1.5 when suitable corrections to the method are applied.

INTRODUCTION

For simple straight-through duct geometries, where a straight line exists from source to detector, the dependence of the intensity of fast neutrons (MeV energies) on duct length can be explained on the basis of a line-of-sight analysis in which no allowance for scattering from the duct walls is made. This dependence has been demonstrated experimentally by Benenson and Shimamoto (ref. 1), Shore and Schamberger (ref. 2), and,

more recently, by Piercey and Bendall (ref. 3), all of whom used sulfur foils to measure the fast-neutron flux emerging from air-filled ducts in water and compared the results with a line-of-sight calculation with good agreement. These comparisons were based on rather idealized geometries where the axial-duct centerline was chosen to coincide with the source centerline, and the terminal end of the duct was placed as close as possible to the source volume to minimize the effect of material attenuation. In addition, no neutron-attenuating material was present inside the duct. Thus, the agreement between theory and experiment has not been verified for a complex reactor-beamhole geometry where off-axis ducts and considerable thicknesses of neutron shielding are present.

As part of a radiation effects program at the NASA Lewis Research Center, calculations and measurements of the fast-neutron flux emerging from a horizontal reactor beamhole have been made. The measurements were taken in Quadrant B of the NASA Plum Brook Reactor, and the calculations were performed with the QAD, line-of-sight, digital computer code (ref. 4).

CORE-BEAMHOLE GEOMETRY

As shown in figure 1(a), the HB-6 beamhole is a nominal 15-inch- (38 cm) diameter aluminum thimble, with a length-to-diameter ratio of 10, which opens to Quadrant B, penetrates the concrete reactor shield, and terminates about 1/2 inch (1 cm) from the beryllium blocks of the primary reflector. The beamhole is surrounded by a shield liner consisting of three sections. At the core end of the HB-6, the liner is composed of alternate layers of iron and water, which also act as thermal shields. The central shield liner is high-density concrete, and the outer section is a mixture of steel shot and water. Located within the thimble is a cylindrical, compartmentalized, aluminum tank that can be flooded selectively to vary the proportions of fast and thermal flux emerging into the quadrant. The offset of the HB-6 axial-duct centerline from the core centerline can be seen in figure 1(b). Also shown are the other test holes contributing to the complexity of the geometry.

ANALYSIS OF CALCULATIONAL TECHNIQUES

Fast-neutron dose rates (which were subsequently converted to fast fluxes) were calculated with the QAD digital computer program, which divides the source volume into a number of smaller volumes, each of which is treated as a point isotropic source. The code then computes the distance through all regions intercepted by the line-of-sight from

a source point to the desired detector point. Neutron attenuation is calculated with the Albert-Welton point kernel (ref. 5).

The use of removal theory was assumed to be valid for the core-beamhole geometry even though very little water or hydrogenous moderator follows the beryllium reflector. Justification for this assumption was based on experimental evidence gathered by Broder, et al. (ref. 6), who examined the possibility of generalizing the removal cross-section method and applied it to hydrogen-free moderators with good results. Specifically, they found that removal cross sections for many substances were insensitive to the moderator material up to an atomic weight of 27 (aluminum). The presence of a low-molecular-weight component in a shield array, therefore, appears to be sufficient justification for the use of removal theory.

An important modification of the neutron attenuation calculation was the use of a collimated beryllium removal cross section as opposed to the conventional broad-beam removal cross section. Only the beryllium cross section was modified because the reflector was the major neutron attenuator between the core and the HB-6 duct. The use of a collimated removal cross section for this geometry can be justified both theoretically and experimentally.

When a broad-beam removal cross section is used to calculate neutron attenuation, the resultant dose rate consists of both a direct and scattered component. The direct component includes neutrons that are essentially uncollided or have undergone very small-angle scattering collisions. The scattered component consists of neutrons that have undergone large-angle elastic scattering or are inelastically scattered and have not lost sufficient energy to lie below the response of a fast-neutron detector. Albert-Welton kernel calculations, using broad-beam removal cross sections, show good agreement with experimental results when the dose contribution of the scattered component is large compared with that of the direct component; for example, when dose measurements are made in a relatively dense medium such as water at distances greater than 4 to 5 mean free paths (about 40 cm) from the shield surface. When measurements are made in a less dense air medium at distances of the order of 10 to 50 feet (3 to 15 m) (about 0.02 to 0.1 mean free paths) from the shield surface, the direct component becomes prominent while the scattered portion is reduced considerably. Consequently, the use of broad-beam removal cross sections can result in overestimated dose rates.

This argument has been examined by Moteff (ref. 7), who compared conventional Albert-Welton calculations using broad-beam removal cross sections with measurements in the Outside Test Tank (OTT) of the Ground Test Reactor (GTR). Both hydrogenous and nonhydrogenous shield arrays were considered for source-detector distances of 9, 13, and 50 feet (2.7, 4, and 15.2 m) in air. The hydrogenous shield consisted of 2 inches (5 cm) of lead, 3 inches (7.6 cm) of beryllium oxide, and 16 inches (41 cm) of lithium hydride; the nonhydrogenous array was composed of 2 inches (5 cm) of lead

TABLE I. - COMPARISON OF CALCULATED (ALBERT-WELTON BROAD BEAM) AND EXPERIMENTAL NEUTRON DOSE RATES[a]

Detector position		Average ratio[b] for shield configuration	
ft	m	Hydrogenous	Nonhydrogenous
9	2.7	3.66	6.00
13	4	5.48	10.5
50	15.2	9.54	20.9

[a]Data from ref. 7.

[b]Calculated dose rate/experimental dose rate.

followed by 22 inches (56 cm) of beryllium. Comparison of conventional Albert-Welton calculations with measurements was reported as the ratio of calculated dose rate to the dose rate measured in the Outside Test Tank. The average ratios for the hydrogenous and nonhydrogenous configurations have been tabulated in table I for presentation herein.

Although the ratios for the hydrogenous shield array are too high by factors of 5.5 to 9.5 at 13 and 50 feet (4 and 15.2 m), respectively, they are not as sensitive as the nonhydrogenous cases where the factors are 10.5 and 20.9. Also presented by Moteff, but not included herein, are the ratios based on a two-component theory calculation, which are shown to be within factors of 1.5 of the experimental data for all shield arrays. The direct-beam component of Moteff's two-component theory results was calculated with the Albert-Welton kernel using collimated removal cross sections and, according to reference 7, accounted for 90 percent of the total dose at 13 and 50 feet (4 and 15.2 m). It is reasonable to infer, therefore, that the use of collimated removal cross sections has been verified experimentally when measurements are made in air at distances of the order of 0.02 to 0.1 mean free paths.

In the case of the HB-6 beamhole, the ratio of the neutron attenuation (due to the beryllium reflector) with collimated removal cross sections to the attenuation calculated with broad-beam removal cross sections was 6.46. (The calculated ratio was based on a broad-beam removal cross section of 1.07 b/atom (1.07×10^{-10} am^2/atom) and a collimated removal cross section value of 1.40 b/atom (1.40×10^{-10} am^2/atom). Both values were obtained from ref. 5.) This ratio was used as a correction factor applied to the Albert-Welton broad-beam dose rates calculated with the QAD code. These integral fast-neutron dose rates have been defined as having a specific lower energy limit to provide a basis of comparison with measurements. Because the QAD code output is in terms of dose rate, conversion to flux was required. The method used herein was to average the multiple-collision Snyder-Neufeld flux-to-dose conversion factors (ref. 8) over both a Watt fission and beryllium-altered fission spectrum. The beryllium spectrum

corresponded to a shield thickness of 90 grams per square centimeter, which was the approximate thickness of the reflector. It should be noted that the use of multiple-collision, rather than single-collision (ref. 9), conversion factors may result in some underestimate of the neutron flux because of the greater magnitude of the Snyder-Neufeld response curve. A discussion of whether the multiple- or single-collision response curve is the proper one to be used for measurements in air or water has been given by Goldstein (ref. 10) and will not be examined herein.

It is of interest to note the variation of the energy-averaged Snyder-Neufeld conversion factor with choice of spectrum. The conversion factor obtained by using the fission spectrum was 18 percent lower than that derived for fission neutrons attenuated by the beryllium reflector. This difference was probably due to the relative hardening of the fission spectrum when altered by beryllium combined with the monotonically increasing response of the Snyder-Neufeld curve with energy. The spectral hardening effect is shown in figure 2 where the two spectra are compared. Both curves have been normalized to the same total source strength. A sharp decrease occurs in the number of neutrons having an energy between 2 and 4 MeV (0.32 and 0.64 pJ), and the peak of the beryllium spectrum has shifted to a higher energy by comparison with the position of the fission spectrum.

Calculated fast-neutron fluxes were based on a nominal reactor power level of 60 megawatts with a core power distribution corresponding to a control rod position of 27.8 inches (70.6 cm) (ref. 11) and a flooded condition in the HT-1 duct.

ANALYSIS OF MEASURED FLUX DATA

Measured fast-neutron fluxes (unpublished data obtained by J. M. Bozek, LRC) are not directly comparable to the QAD code results because of the difference in the lower energy limit of their flux integrals. Measured fluxes which are based on a sulfur energy threshold of 2.48 MeV (0.397 pJ) were extrapolated to a lower energy limit of 0.3 MeV (0.048 pJ) (assuming both a fission and a beryllium spectrum) to provide a basis of comparison with the calculated results. Because the accepted effective energy range of the Albert-Welton kernel is fast, that is, a lower energy limit of 0.1 to 1 MeV (0.016 to 0.16 pJ) , a reasonable choice would be 0.3 MeV (0.048 pJ). Assumption of a different lower energy limit could decrease the extrapolated value of measured flux by as much as a factor of 1.4 (for E_{min} = 1 MeV (0.16 pJ)).

Extrapolation of measured results to an energy of 0.3 MeV (0.048 pJ) was accomplished by using both the Watt fission spectrum and a beryllium-modified (90 g/cm^2) spectrum obtained from moments method calculations (ref. 12). These two spectra were chosen to represent the possible extremes of the true HB-6 duct spectrum, which was

estimated to be a somewhat hardened fission spectrum caused by absorption of low-energy neutrons in the beryllium reflector. The effect of spectral hardening in the fast region was shown in figure 2.

The measured standardized flux for neutrons with energies greater than 2.48 MeV (0.379 pJ) was $8.2\times10^{6}\pm35$ percent neutrons per square centimeter per second based on a fission spectrum. The standardized flux was based on a fixed set of core operating parameters, and the flux at other operating parameters may be obtained by applying a set of correction factors. Because the experimental data were based on the assumption of a fission spectrum, conversion of the measured flux data to a beryllium spectrum required that an effective energy threshold and average cross section be calculated to interpret the sulfur foil data. This cross section and energy threshold were calculated (see appendix) to be 0.271 barn and 2.98 MeV (0.477 pJ), while that used for a fission spectrum, was 0.206 barn and 2.48 MeV (0.379 pJ) (ref. 13). The beryllium spectrum standardized flux for neutrons with energies greater than 2.48 MeV (0.397 pJ) was then found to be $6.8\times10^{6}\pm35$ percent neutrons per square centimeter per second. The standardized flux for neutrons with energies greater than 0.3 MeV (0.048 pJ) was calculated by multiplying the standardized flux for neutrons with energies greater than 2.48 MeV (0.397 pJ) by the ratio of the fraction of neutrons above 2.48 MeV for both spectra. An analysis of all the calculations described in this section is given in the appendix.

RESULTS AND DISCUSSION

The results of the comparison of measured and calculated fast neutron fluxes emerging from the HB-6 duct are presented in figure 3 in terms of spatial variation along the projected vertical centerline of the HB-6 duct for 0, 3, and 6 inches (0, 7.6, and 15.2 cm) of water in the duct. Calculated values are shown as dashed lines along a vertical traverse of the projected duct centerline while measured fluxes have been averaged over four arbitrary duct regions. Experimental data are presented for both fission and beryllium spectral assumptions.

The tendency of the spatial variation of the fast flux to peak at the upper region of the duct is reflected in both the measured and calculated results. The reason for this effect, however, is not understood. Within the accuracy of the calculational method (line-of-sight, removal theory) the maximum deviation between extrapolated measured fast flux and calculation was a factor of 1.5 ± 0.5. Uncertainty of both the actual neutron

spectrum emerging from the duct and lower energy limit of the calculational method was probably the most significant source of difference in the comparison.

Lewis Research Center,
National Aeronautics and Space Administration,
Cleveland, Ohio, April 7, 1967,
120-27-06-07-22.

APPENDIX - SUMMARY OF CALCULATIONS REQUIRED TO ANALYZE MEASURED FLUX DATA

Calculation of Effective Energy Threshold and Average Cross Section For Beryllium-Altered Fission Spectrum

The saturated activity of a foil exposed to a neutron flux is

$$A = \int_0^\infty \varphi(E)\sigma(E)dE \tag{A1}$$

where $\varphi(E)$ and $\sigma(E)$ are the energy dependent neutron flux and activation cross section, respectively. It is more convenient to write equation (A1) as

$$A = \overline{\sigma}_{eff}\int_{E_t}^\infty \varphi(E)dE \tag{A2}$$

This form reduces from equation (A1) when the cross section $\sigma(E)$ has a threshold E_t, below which it is zero, and above which the constant value $\overline{\sigma}_{eff}$ exists. Even when the cross section has a more general and realistic energy dependence, however, equation (A2) is equivalent to equation (A1) as long as a flux spectrum can be approximated over the energy range where the foil cross section is significant. Here $\overline{\sigma}_{eff}$ and E_t are parameters to be so determined that equation (A2) yields precisely the same value as equation (A1). Under these conditions, $\overline{\sigma}_{eff}$ and E_t may not have such obvious physical interpretations as existed in the step-function assumption.

The method used in reference 13 provides a prescription for the calculation of E_t once a spectral shape $\eta(E)$ is assumed.

$$\int_{E_t}^\infty \sigma(E)\eta(E)dE = 0.95\int_0^\infty \sigma(E)\eta(E)dE \tag{A3}$$

The spectral shape is simply defined as the ratio of the energy dependent flux $\varphi(E)$ to some constant flux φ_o, thus,

$$\varphi(E) = \varphi_o\eta(E) \tag{A4}$$

Therefore, equating equations (A1) and (A2) and solving for $\overline{\sigma}_{eff}$ yields

$$\bar{\sigma}_{eff} = \frac{\int_0^\infty \sigma(E)\varphi(E)dE}{\int_{E_t}^\infty \varphi(E)dE} \tag{A5}$$

A tabulation of the quantities needed to solve equations (A5) and (A3) is given in table II for a fission spectrum altered by 90 gram-per-square-centimeter beryllium. Application of equation (A3) yields an effective threshold energy of 2.98 MeV for a sulfur foil placed in a beryllium spectrum. Calculation of $\bar{\sigma}_{eff}$ from equation (A5) yields a value of 0.271 barn.

Calculation of Standardized Flux of Neutrons with Energy Above 2.48 MeV (0.397 pJ) in Beryllium Spectrum

The standardized flux of neutrons with energy above 2.48 MeV (0.397 pJ) in a beryllium-altered (90 g/cm^2) spectrum was calculated by the methods described previously. Rewriting equation (A5) to yield the flux gives

$$\int_{E_t}^\infty \varphi(E)dE = \frac{A}{\bar{\sigma}_{eff}} \tag{A6}$$

Both E_t and $\bar{\sigma}_{eff}$ have been calculated, and the measured activation rate A was 1.69×10^{-18} disintegration per second. The standardized flux for neutrons with energy above E_t (2.98 MeV (0.477 pJ)) was then calculated from equation (A6) as follows:

$$\int_{2.98}^\infty \varphi(E)dE = \frac{1.69\times10^{-18}\ \text{n/sec}}{(0.271\ \text{b})(10^{-24}\ \text{cm}^2/\text{b})} = 6.2\times10^6\ \text{neutrons}\ (\text{cm}^2)(\text{sec})$$

This flux was extrapolated to a lower energy limit of 2.48 MeV (0.397 pJ) (actually 2.44 MeV (0.391 pJ)) from the data given in table II and the following general equation:

$$\int_{E_1}^\infty \varphi(E)dE = \frac{F(E_1)}{F(E_2)} \cdot \int_{E_2}^\infty \varphi(E)dE \tag{A7}$$

where F(E) is the fraction of neutrons with energy above E (see next section). Applying equation (A7) yields the standardized beryllium flux:

TABLE II. - DATA TABULATION FOR 90 GRAMS PER SQUARE CENTIMETER BERYLLIUM SPECTRUM

(a) U.S. customary units

Minimum energy, E_{min}, MeV	Energy decrement, ΔE, MeV	Differential number flux, $\varphi(E)$, (neutrons/sec)(MeV) (a)	Number flux of neutrons with energies between E and E + ΔE, $\varphi(E)\Delta E$, neutrons/sec (b)	Energy dependent activation cross section, $\sigma(E)$, b (c)	Activation due to neutrons of energy E in range ΔE, $\varphi(E)\sigma(E)\Delta E$, (neutrons/sec)/(barns) (d)
14.75	3.25	2.15×10^{-7}	6.99×10^{-7}	0.242	1.69×10^{-7}
12.1	2.65	1.22×10^{-6}	3.23×10^{-6}	.358	1.16×10^{-6}
9.89	2.21	8.07×10^{-6}	1.78×10^{-5}	.389	6.92×10^{-6}
8.10	1.79	2.16×10^{-5}	3.87×10^{-5}	.337	1.31×10^{-5}
6.63	1.47	4.5×10^{-5}	6.61×10^{-5}	.336	2.22×10^{-5}
5.43	1.20	1.18×10^{-4}	1.41×10^{-4}	.258	3.64×10^{-5}
4.44	.99	1.83×10^{-4}	1.81×10^{-4}	.307	5.55×10^{-5}
3.64	.80	1.81×10^{-4}	1.44×10^{-4}	.221	3.18×10^{-5}
2.98	.66	1.21×10^{-4}	7.99×10^{-5}	.112	8.91×10^{-6}
2.69	.29	8.13×10^{-5}	2.36×10^{-5}	.0722	1.70×10^{-6}
2.44	.25	1.83×10^{-4}	4.5×10^{-5}	.0583	2.62×10^{-6}
2.00	.44	7.68×10^{-4}	3.38×10^{-4}	.00560	1.89×10^{-6}
1.63	.37	1.03×10^{-3}	3.81×10^{-4}	0	0

(b) SI units

Minimum energy, E_{min}, pJ	Energy decrement, ΔE, pJ	Differential number flux, $\varphi(E)$, (neutrons/sec)(pJ) (a)	Number flux of neutrons with energies between E and E + ΔE, $\varphi(E)\Delta E$, neutrons/sec (b)	Energy dependent activation cross section, $\sigma(E)$, am^2 (c)	Activation due to neutrons of energy E in range ΔE, $\varphi(E)\sigma(E)\Delta E$, (neutrons/sec)($am^2$) (d)
2.36	0.521	1.34×10^{-6}	6.99×10^{-7}	2.42×10^{-11}	1.69×10^{-17}
1.94	.424	7.62×10^{-6}	3.23×10^{-6}	3.58	1.16×10^{-16}
1.58	.354	5.04×10^{-5}	1.78×10^{-5}	3.89	6.92×10^{-16}
1.30	.287	1.35×10^{-4}	3.87×10^{-5}	3.37	1.31×10^{-15}
1.06	.235	2.81×10^{-4}	6.61×10^{-5}	3.36	2.22×10^{-15}
.870	.192	7.36×10^{-4}	1.41×10^{-4}	2.58	3.64×10^{-15}
.711	.158	1.14×10^{-3}	1.81×10^{-4}	3.07	5.55×10^{-15}
.583	.128	1.13×10^{-3}	1.44×10^{-4}	2.21	3.18×10^{-15}
.477	.106	7.55×10^{-4}	7.99×10^{-5}	1.12	8.91×10^{-16}
.431	.0464	5.07×10^{-4}	2.36×10^{-5}	.722	1.70×10^{-16}
.391	.0400	1.14×10^{-3}	4.5×10^{-5}	.583	2.62×10^{-16}
.320	.0705	4.79×10^{-3}	3.38×10^{-4}	.056	1.89×10^{-16}
.261	.0593	6.43×10^{-3}	3.81×10^{-4}	0	0

[a] $\varphi(E)$ corresponds to $4\pi R^2 N_0(r,E)$ used in ref. 10.

[b] $\sum_{2.44}^{\infty} \varphi(E)\Delta E = 7.4\times10^{-4}$ and $\sum_{2.98}^{\infty} \varphi(E)\Delta E = 6.72\times10^{-4}$.

[c] Cross-section data obtained from tabulation in ref. 13.

[d] $\sum_{0}^{\infty}\varphi(E)\sigma(E)\Delta E = 1.82\times10^{-4}$.

TABLE III. - RATIOS OF FRACTION OF NEUTRONS ABOVE 0.3 MeV (0.048 PICOJOULE) TO THOSE ABOVE 2.48 MeV (0.397 PICOJOULE) FOR FISSION AND BERYLLIUM SPECTRA[a]

Spectrum	Fraction of neutrons above 0.3 MeV, MeV (pJ)	Fraction of neutrons above 2.48 MeV, MeV (pJ)	Fraction ratio, $F(E_2)/F(E_1)$, F(0.3 MeV)/F(2.48 MeV)
Fission	0.93 (0.149)	0.29 (0.046)	3.15
Beryllium ($90\ g/cm^2$)	1.00 (.160)	.34 (.054)	2.95

[a]Data calculated from ref. 10.

$$\int_{2.48}^{\infty} \varphi(E)dE = \left(\frac{7.4\times10^{-4}}{6.72\times10^{-4}}\right)\left(6.2\times10^{6}\right) = 6.8\times10^{6}\ \text{neutrons}/(\text{cm}^2)(\text{sec})$$

Calculation of Standardized Flux of Neutrons with Energy Above 0.3 MeV (0.048 pJ) in Fission and Beryllium Spectrum

Let N(E) be the fraction of neutrons at E per MeV(pJ) interval, that is, the differential spectrum. Then, following the notation in Goldstein (ref. 10), we can define F(E) as the fraction of neutrons with energy above E:

$$F(E) = \int_{E}^{\infty} N(E')dE'$$

In general, the flux of neutrons with energy above E_1 may be extrapolated to give the flux of neutrons above some other energy E_2 by multiplying the flux above energy E_1 by the ratio $F(E_2)/F(E_1)$ for a given (or assumed) spectrum.

The values of $F(E_1)$ and $F(E_2)$ and their quotient for E_1 = 2.48 MeV (0.397 pJ) and E_2 = 0.3(0.048 pJ) MeV are given in table III for both a fission and a beryllium spectrum. All data were calculated from results of moments method calculations given in reference 10.

The standardized fission-spectrum flux of neutrons with energy above 0.3 MeV (0.048 pJ) is

$$\varphi(E > 0.3 \text{ MeV}) = (8.2\times10^{6})(3.15) = 2.6\times10^{7} \text{ neutrons/(cm}^{2})\text{(sec)}$$

and the standardized beryllium-spectrum flux of neutrons with energy above 0.3 MeV (0.048 pJ) is

$$\varphi(E > 0.3 \text{ MeV}) = (6.8\times10^{6})(2.95) = 2.0\times10^{7} \text{ neutrons/(cm}^{2})\text{(sec)}$$

REFERENCES

1. Benenson, R. E.; and Shimamoto, Y.: Ray Analysis of the Transmission of Fast Neutrons Through Cylindrical Ducts in Water. Reactor Shielding Information Meeting, Part 3, Engineer-Research and Development Laboratories, Fort Belvoir, Virginia, May 12-13, 1955. AEC Rep. No. WASH-292 (Pt. 3), Sept. 1955, pp. 64-73.

2. Shore, F. J.; and Schamberger, R. D.: The Transmission of Neutrons Through Ducts in Water. Rep. No. BNL-390, Brookhaven National Labs., Mar. 1, 1956.

3. Piercey, D. C.; and Bendall, D. E.: The Transmission of Fast Neutrons Along Air Filled Ducts in Water. Rep. No. AEEW-R 69, United Kingdom Atomic Energy Authority, June 1962.

4. Malenfant, Richard E.: QAD: A Series of Point-Kernel General-Purpose Shielding Programs. Rep. No. LA-3573, Los Alamos Scientific Lab., Apr. 1967.

5. Blizard, E. P., ed.: Shielding. Vol. III, Part B of Reactor Handbook. Second ed., Interscience Publishers, 1962.

6. Broder, D. L.; Kutuzov, A. A.; Levin, V. V.; and Frolov, V. V.: Use of the Method of "Removal Cross Section" for the Computation of Shielding Not Containing Hydrogen. NASA TT F-10155, 1966.

7. Moteff, J.: Proposed Two-Component Method of Nuclear Shield Analysis. Rep. No. DC 60-4-87, General Electric Co., Apr. 13, 1960.

8. Anon: Protection Against Neutron Radiation up to 30 Million Electron Volts. Handbook No. 63, National Bureau of Standards, Nov. 22, 1957.

9. Anon.: Measurement of Absorbed Dose of Neutrons and of Mixtures of Neutrons and Gamma Rays. Handbook No. 75, National Bureau of Standards, Feb. 3, 1961.

10. Goldstein, Herbert: Fundamental Aspects of Reactor Shielding. Addison-Wesley Pub. Co., 1959.

11. Giesler, Harold W.; Reilly, Harry J.; and Poley, William A.: Low-Power Test of the Plum Brook Reactor. NASA TN D-1560, 1963.

12. Goldstein, H.; and Mechanic, H.: Penetration of Neutrons From a Point Fission Source Through Beryllium and Beryllium Oxide. Rep. No. NDA 2092-9, Nuclear Development Corp. of America, June 23, 1958.

13. Barrall, R. C.; and McElroy, W. N.: Neutron Flux Spectra Determination by Foil Activation. Vol. II. Experimental and Evaluated Cross Section Library of Selected Reactions. Rep. No. TDR-W6085-4-Vol. 2 (AFWL TR-65-34-Vol. 2, DDC No. AD-470470), IIT Research Institute, Aug. 1965.

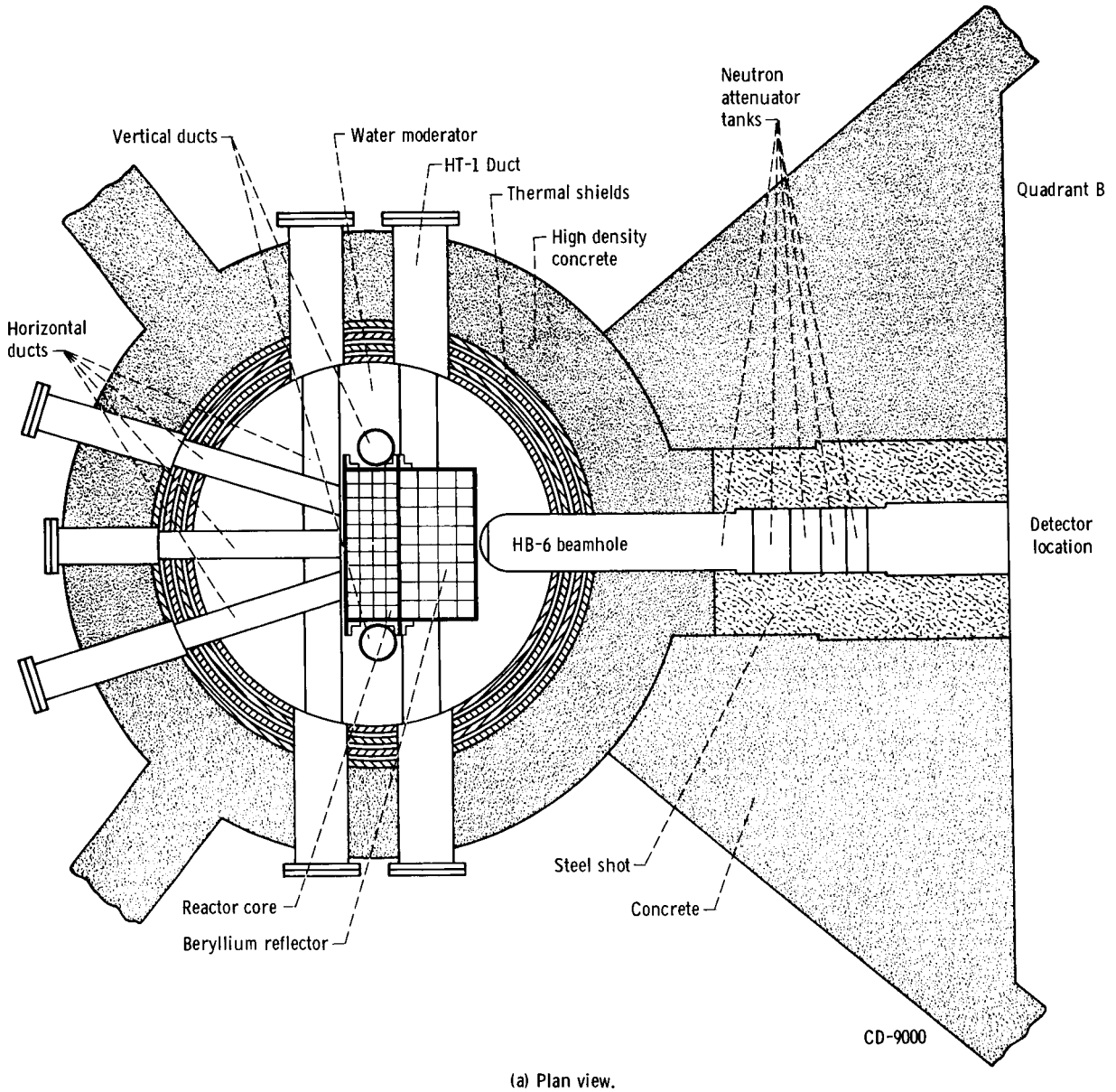

(a) Plan view.

Figure 1. - Core-beamhole assembly at HB-6 horizontal duct centerline.

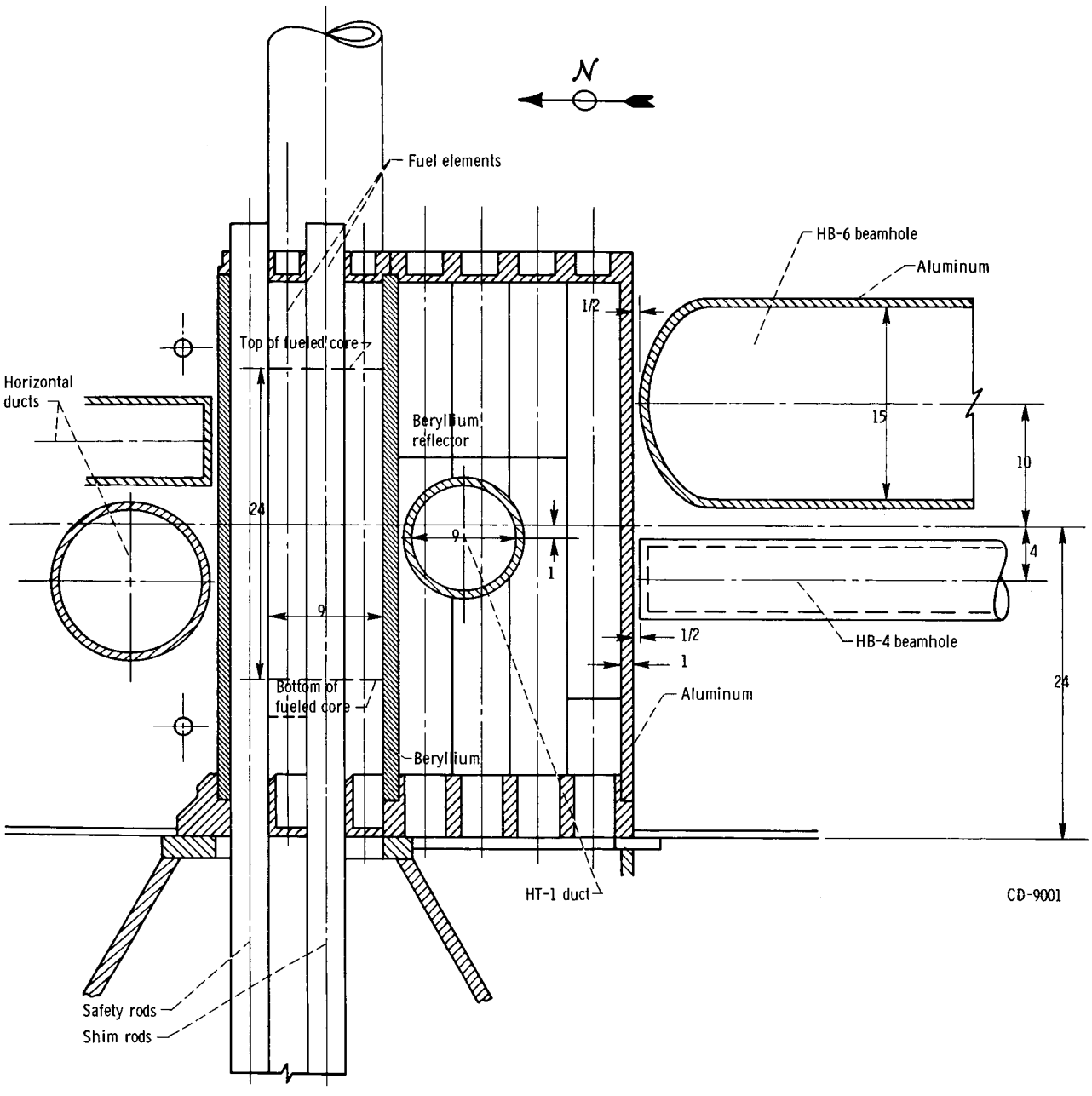

(b) Side view. (Dimensions in inches.)

Figure 1. - Concluded.

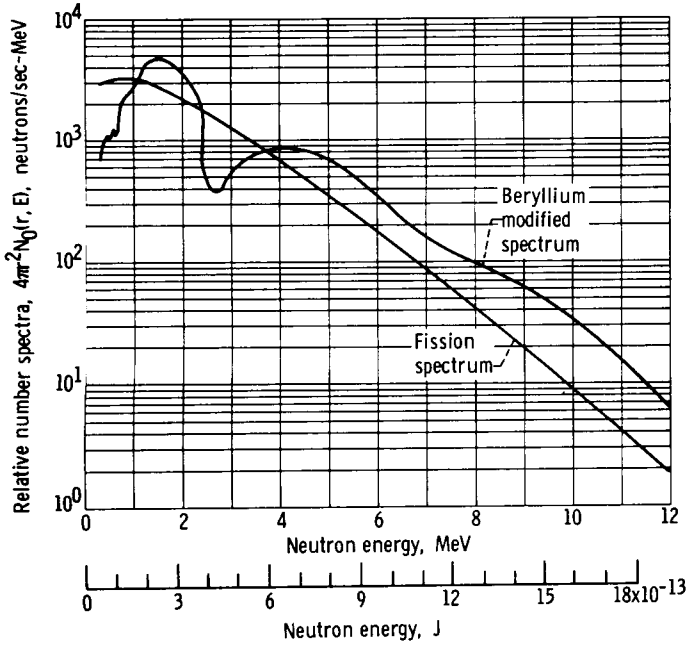

Figure 2. - Normalized differential spectra of fission neutrons and fission neutrons attenuated by 90-gram-per-square-centimeter beryllium. (Beryllium spectrum from ref. 12.)

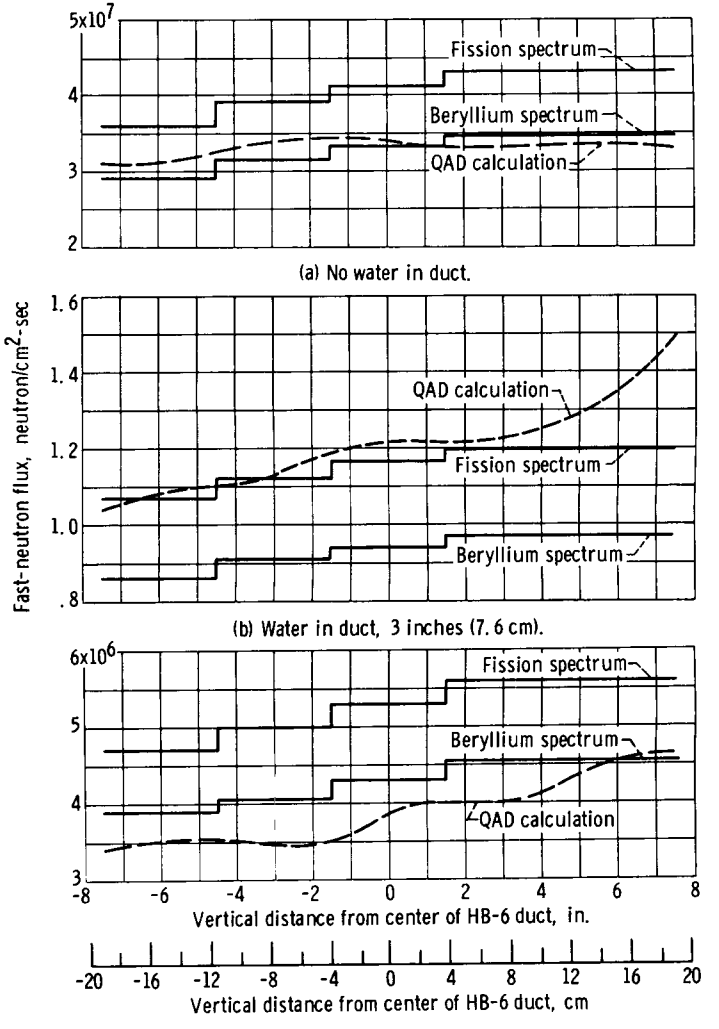

Figure 3. - Comparison of measured and calculated fast-neutron fluxes emerging from HB-6 beamhole. Energy, greater than 0.3 MeV (0.048 pJ).